Supplemental information

Mapping vestibular and visual contributions

to angular head velocity tuning in the cortex

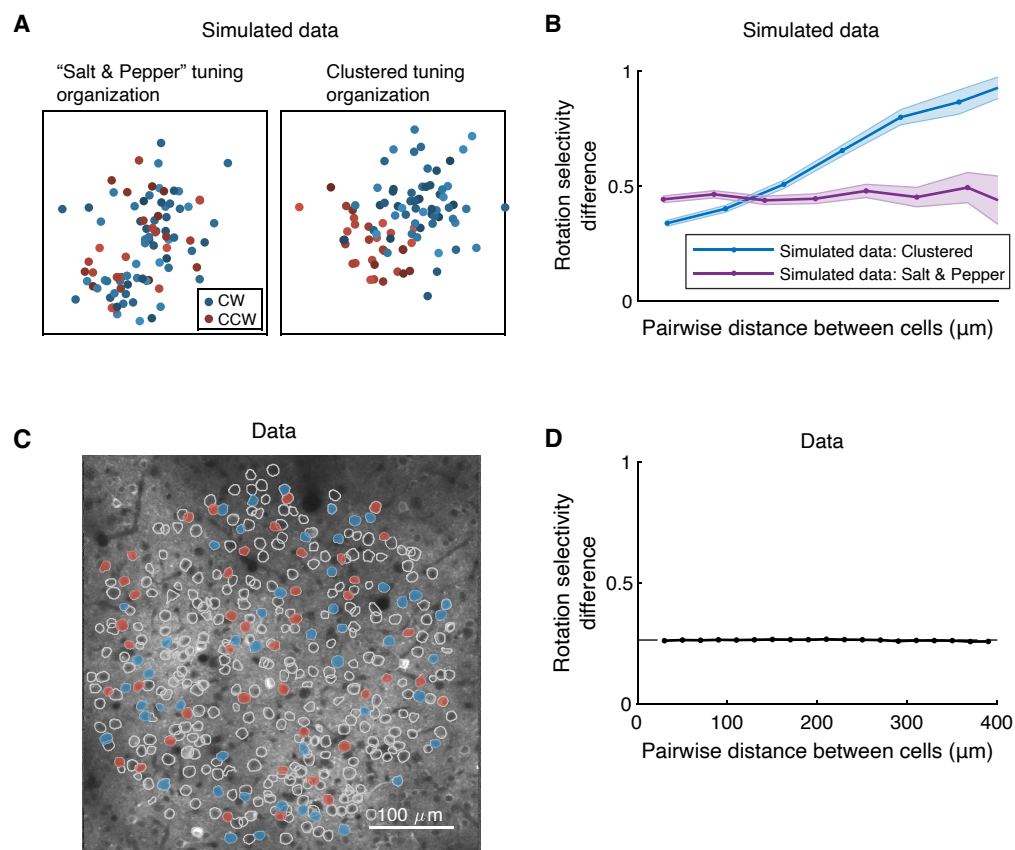Eivind Hennestad, Aree Witoelar, Anna R. Chambers, and Koen Vervaeke

A Simulated data

"Salt & Pepper" tuning organization | Clustered tuning organization

CW
CCW

B Simulated data

Rotation selectivity difference

Pairwise distance between cells (µm)

Simulated data: Clustered
Simulated data: Salt & Pepper

C Data

100 µm

D Data

Rotation selectivity difference

Pairwise distance between cells (µm)

Figure S1. Rotation-selective cells are not spatially clustered. (Related to figure 1)

(A) Simulated data showing two hypothetical forms of spatial organization between cells with similar tuning. (Left) A "salt and pepper" organization lacks any spatial correlation between similarly tuned cells. (Right) A "spatially clustered" organization shows neurons with similar tuning properties in closer proximity. Blue and red dots represent CW and CCW-tuned cells, respectively, on a Field of View size (FOV) that matches the typical FOV size used for two-photon imaging.

(B) The relation between rotation selectivity (CW or CCW) difference and physical distance for simulated data. The rotation selectivity difference between cells *i* and *j* defined as $\Delta R_{ij} = |R_i - R_j|$ is averaged on each physical distance bin in the FOV. For a "salt-and-pepper" organization, this measure is not dependent on the distance between cells. For a "spatially clustered" organization, this measure increases with distance.

(C) Experimental data showing a two-photon microscopy image of an example FOV with rotation-selective cells, color-coded in red (CCW) and blue (CW).

(D) The relation between rotation selectivity difference and physical distance for experimental data resembles more closely a "salt-and-pepper" organization (30 FOVs from 5 mice).
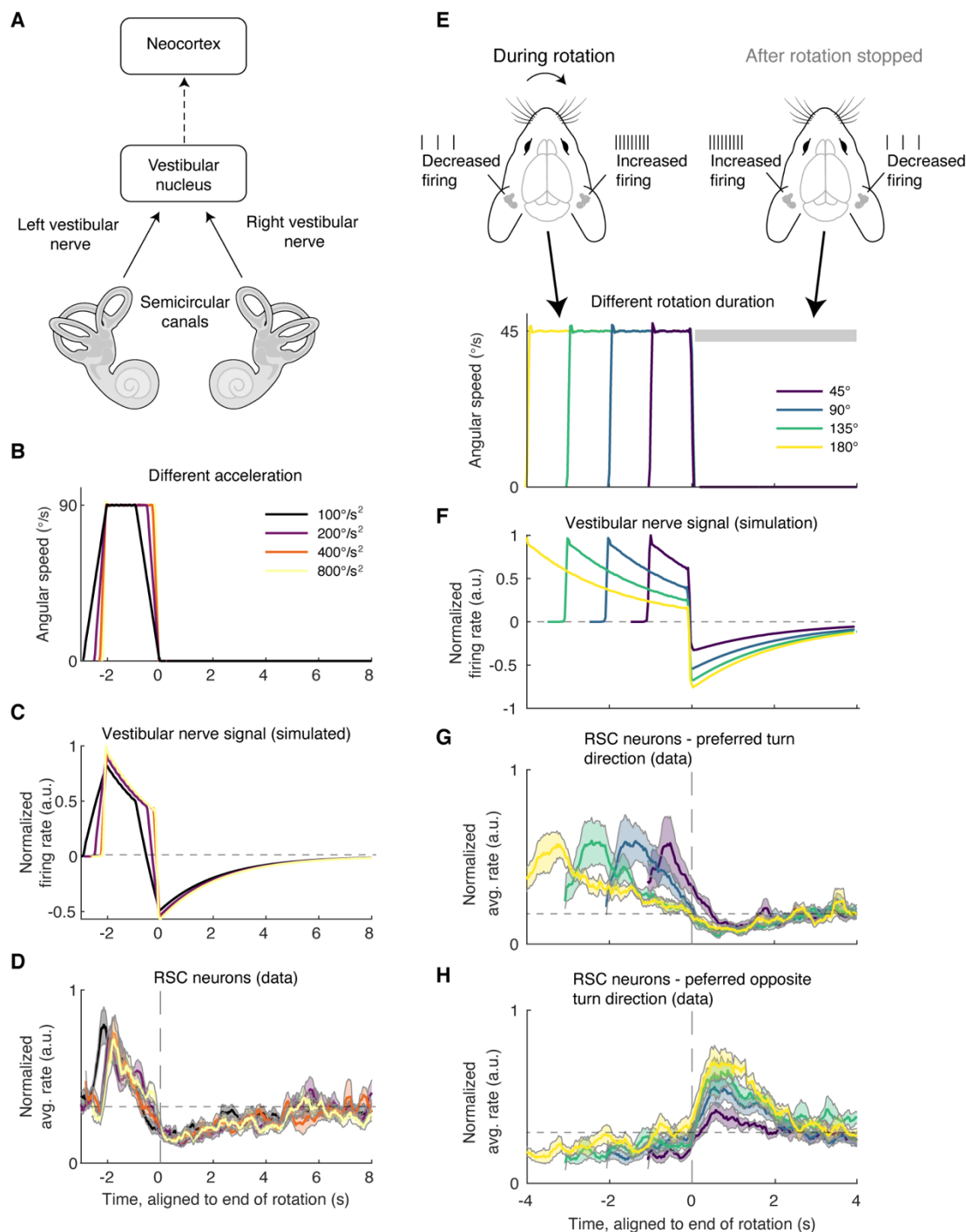
Figure S2. Evidence for a vestibular origin of AHV tuning in RSC. (Related to figure 5)

(A) Schematic showing a simplified pathway from the vestibular organs to the cortex. The afferent fibers of the vestibular nerve convey head motion information from the hair cells in the vestibular organs to the vestibular nucleus in the brain stem. From there on, vestibular information can take different pathways to the neocortex (dashed arrow).

(B) Stimulation protocol: The mouse is briefly rotated at a speed of 90 °/s using different accelerations and decelerations.

(C) Simulations showing the response of afferent fibers in the vestibular nerve using the speed profiles in (B).

(D) Experimental data showing the response of all rotation-selective RSC neurons (average rate $\pm$ s.e.m) using the speed profiles shown in B (594 rotation-selective cells from 4 mice).

(E) Stimulation protocol: The mouse is rotated at a constant speed of 45 °/s for different durations (spanning angles of 45 to 180°). (Left) For brief CW rotations, fibers in the right vestibular nerve will increase firing, while those in the left vestibular nerve will decrease firing. During long rotations, however, the firing rates of both nerves will return to baseline due to the adaptation of the inertia signal in the vestibular organs. (Right) When stopping the mouse after a long CW rotation, the firing rates in the left vestibular nerve will go up and the ones in the right vestibular nerve will go down. This implies that, for long CW rotations, CW-tuned cells respond during rotation, while CCW-tuned cells will respond when the rotation stops.

(F) Simulations showing the response of afferent fibers in the vestibular nerve using the speed profiles in (E).

(G) Experimental data showing the response of all CW-tuned neurons in RSC (average rate $\pm$ s.e.m) using the speed profiles shown in E (330 cells from 4 mice).

(H) Experimental data showing the response of all CCW-tuned neurons in RSC (average rate $\pm$ s.e.m) after the rotation stops (249 cells from 4 mice).
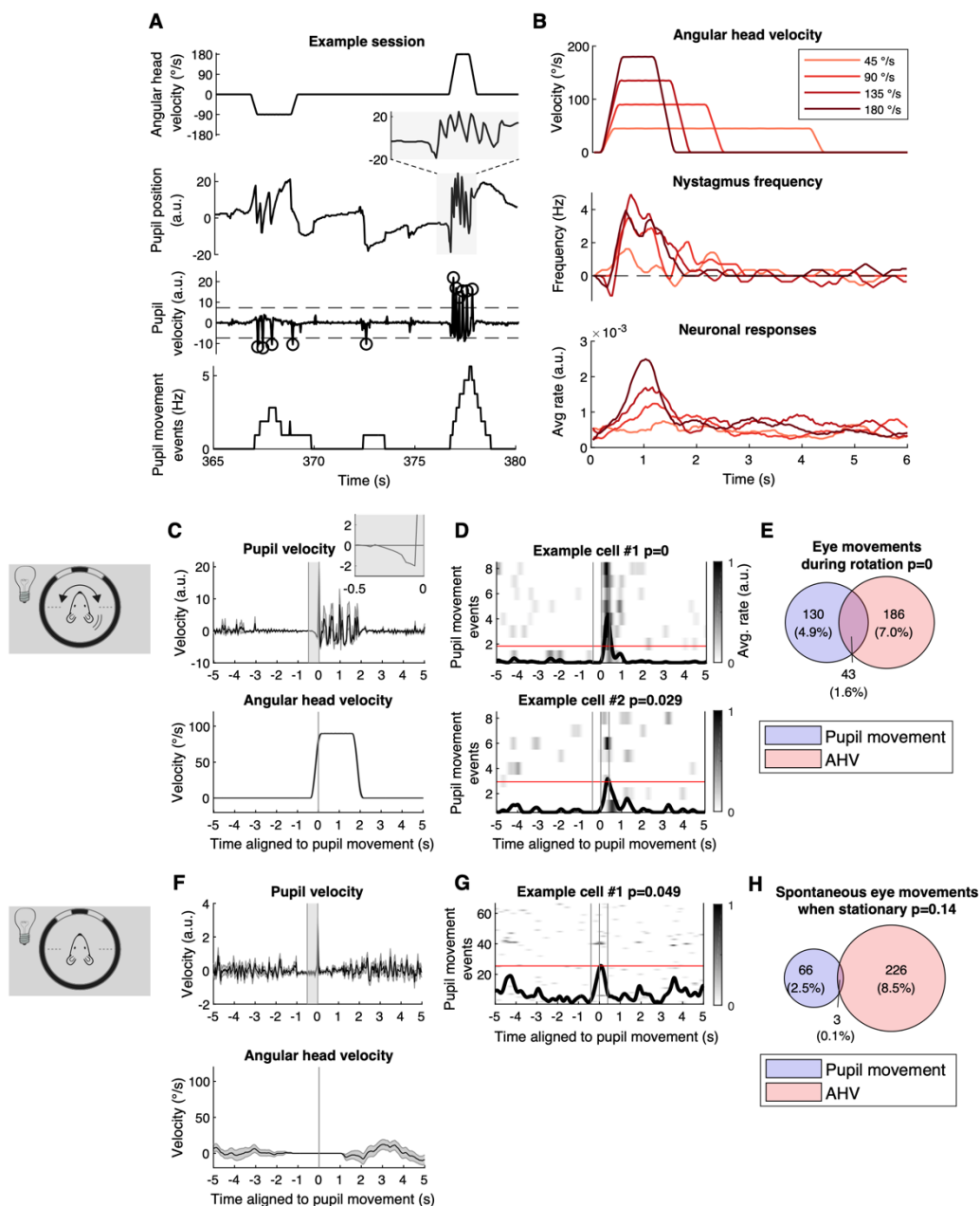
Figure S3. Do RSC neurons encode eye movements? (Related to figure 5)

(A) Example data of a mouse being rotated in CW or CCW directions at different velocities in the dark, while tracking pupil movements and neuronal activity in RSC. The experimental protocol is described in Figure 3A. (1st plot) Angular velocity profile. Example sequence of 2 trials. (2nd plot) Pupil position. Note the nystagmus during rotations (saw-tooth-like eye movements composed of a slow phase and a fast phase). (3rd plot) Pupil velocity (derivative of pupil position). A pupil movement event (circles) was detected when the pupil velocity passed a threshold, defined as velocities exceeding the 95th percentile (two tailed distribution). (4th plot) Pupil movement events were smoothened over a 1-second window to produce the instantaneous frequency.

(B) Comparison of nystagmus beat frequency and neuronal responses in RSC, for one example session. (Top) Angular velocity profile. (Middle) Average nystagmus beat frequency. The nystagmus beat frequency was obtained from the pupil movement event frequency during rotations. (Bottom) Average rate of all RSC neurons in the FOV (287 neurons).

(C) Pupil velocity aligned to the first fast phase of the nystagmus during rotations in the dark. Top: example pupil velocity for 90 °/s trials. Shaded area shows the fast phase of the nystagmus preceded by the slow phase (see inset). Bottom: angular head velocity.

(D) Two example neurons that were significantly modulated during the 1 second window centred on the first fast phase of the nystagmus. Neurons were modulated when their average rate exceeded the 95th percentile of shuffled data (red line).

(E) Venn diagram of AHV cells and cells modulated during the fast or slow phase of the nystagmus (rotations in the dark) (2643 cells from 6 mice, 8 sessions). P-value represents the significance value of overlap compared to random labels.

(F) Pupil velocity aligned to spontaneous pupil movement events when the mouse is stationary. Top: Pupil velocity. Bottom: Angular head velocity.

(G) Example neuron that was significantly modulated during the 1 second window centred on spontaneous pupil movement events (mouse is stationary).

(H) Venn diagram of AHV cells and cells modulated during spontaneous pupil movements when the mouse is stationary.
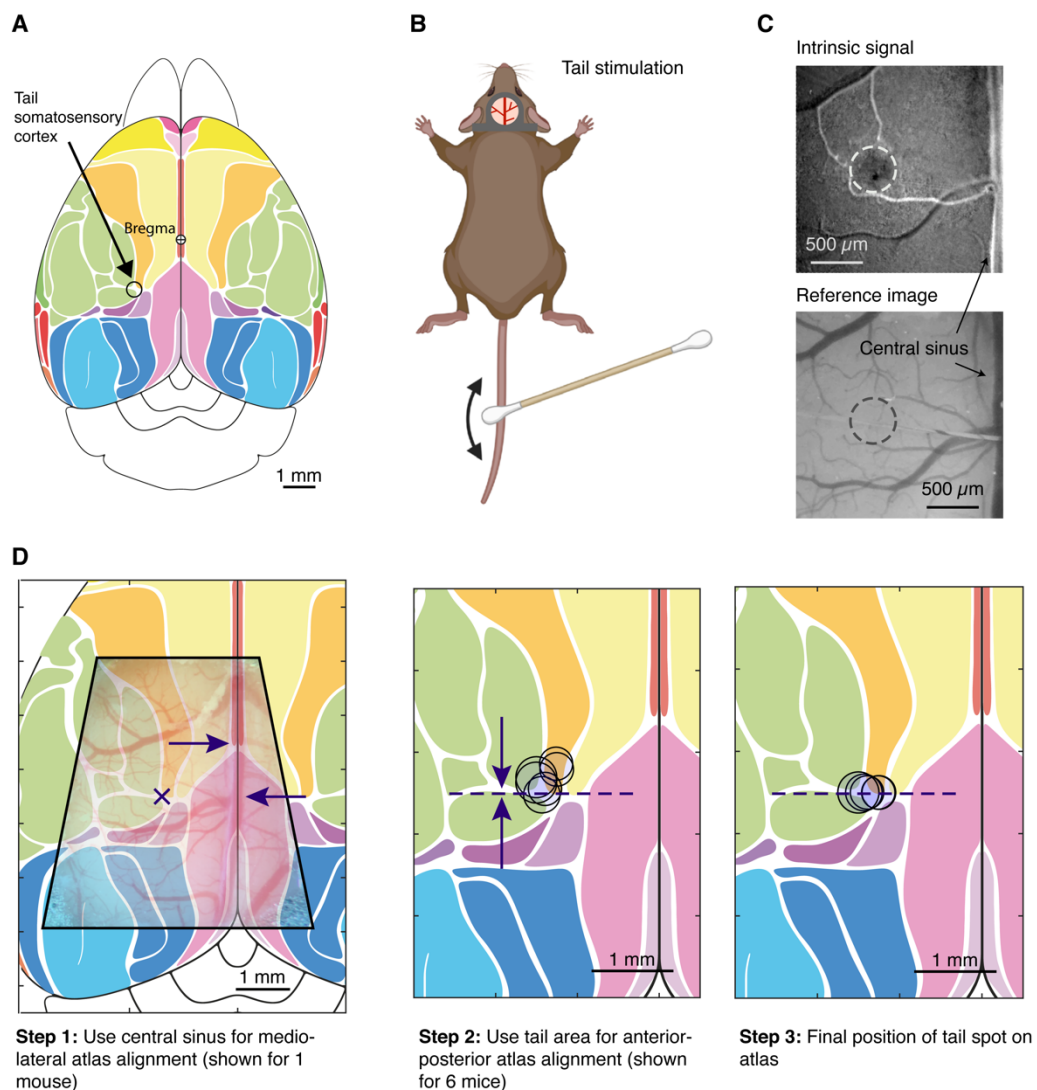
A

Tail somatosensory cortex

Bregma

1 mm

B

Tail stimulation

C

Intrinsic signal

500 µm

Reference image

Central sinus

500 µm

D

Step 1: Use central sinus for medio-lateral atlas alignment (shown for 1 mouse)

1 mm

Step 2: Use tail area for anterior-posterior atlas alignment (shown for 6 mice)

1 mm

Step 3: Final position of tail spot on atlas

1 mm

Figure S4. Intrinsic imaging to align two-photon maps to a reference image of the cortex. (Related to figure 6)

(A) The tail somatosensory cortex is a small ~200-300 µm area, located at the borders of somatosensory cortex S1, primary and secondary motor cortex (S1 and S2) and posterior parietal cortex (PPC). Therefore, identifying this area in every mouse can be used to align two-photon microscopy-generated maps of tuned-neurons to a standardized reference image.

(B) We used a cotton swab to stroke the tail while performing intrinsic imaging.

(C) (Top) Example of intrinsic signal response to tail stimulation. (Bottom) Reference image showing blood vessel pattern.

(D) Procedure to align maps of individual mice to a reference image. (Left) First, the central sinus was used to align maps along the mediolateral axis. (Middle) Next, the location of the tail somatosensory cortex was used to align maps along the anterior-posterior axis. (Right) Final location of the tail somatosensory cortex of individual mice on the reference image.
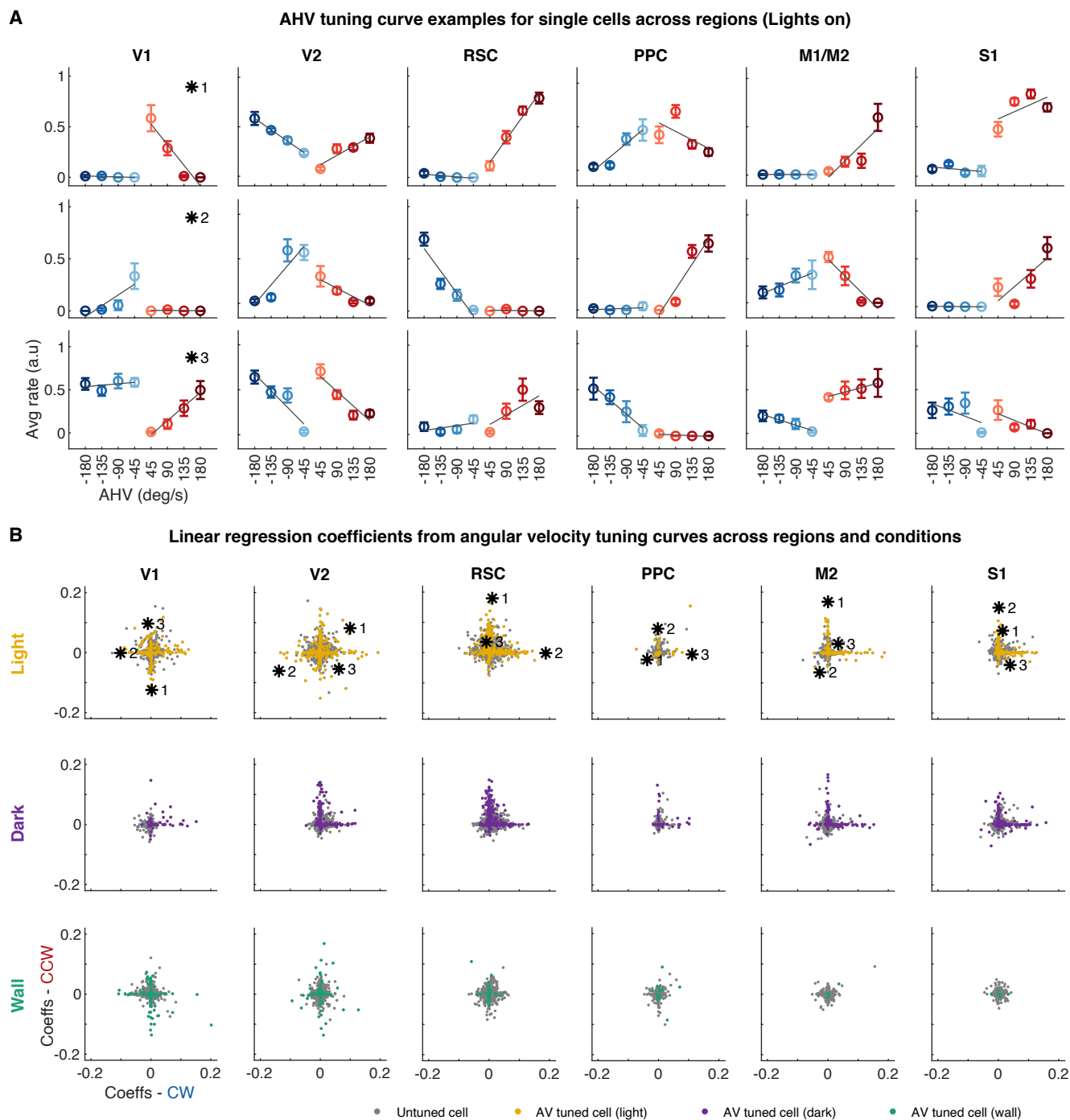
A AHV tuning curve examples for single cells across regions (Lights on)

B Linear regression coefficients from angular velocity tuning curves across regions and conditions

Figure S5. AHV tuning curves across regions and stimulus conditions. (Related to figure 7)

(A) Examples of AHV tuning curves from different cortical areas (obtained using rotations in light). Tuning curves show average rate across all trials (± s.e.m) as a function of angular velocity. The CW (blue) and CCW (red) portions of the tuning curves are fitted independently by linear regression.

(B) Regression slopes of all cells for CW (x-axis) and CCW (y-axis) portions of the AHV tuning curves, shown for different cortical areas and different stimulus conditions. Asterisks correspond to the examples in (A). See captions for Figures 6 and 7 for a detailed list of the number of mice and cells in each plot.
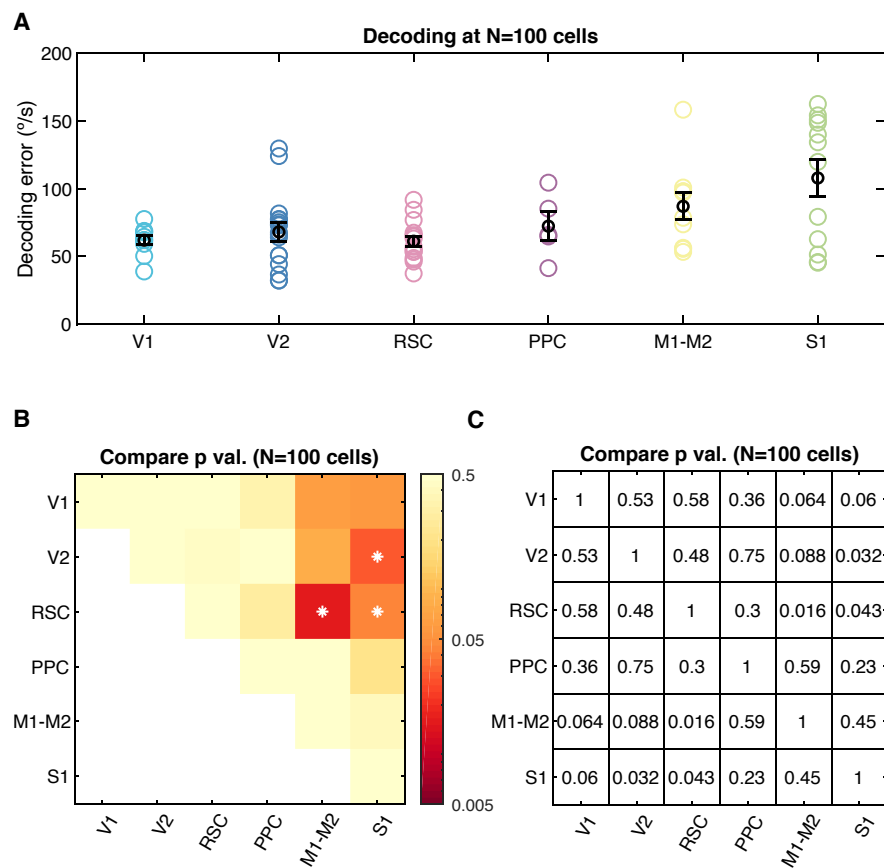
A

Decoding at N=100 cells

B

Compare p val. (N=100 cells)

C

Compare p val. (N=100 cells)

	V1	V2	RSC	PPC	M1-M2	S1
V1	1	0.53	0.58	0.36	0.064	0.06
V2	0.53	1	0.48	0.75	0.088	0.032
RSC	0.58	0.48	1	0.3	0.016	0.043
PPC	0.36	0.75	0.3	1	0.59	0.23
M1-M2	0.064	0.088	0.016	0.59	1	0.45
S1	0.06	0.032	0.043	0.23	0.45	1

Figure S6. Comparison of the decoding error across cortical areas. (Related to figure 6)
(A) Average (± s.e.m) decoding error of multiple cortical areas using a fixed number of randomly selected neurons (N=100).

(B, C) Statistical comparison between cortical areas (Wilcoxon-Mann-Whitney test). See caption of Figure 6 for a detailed list of the number of mice for each plot.
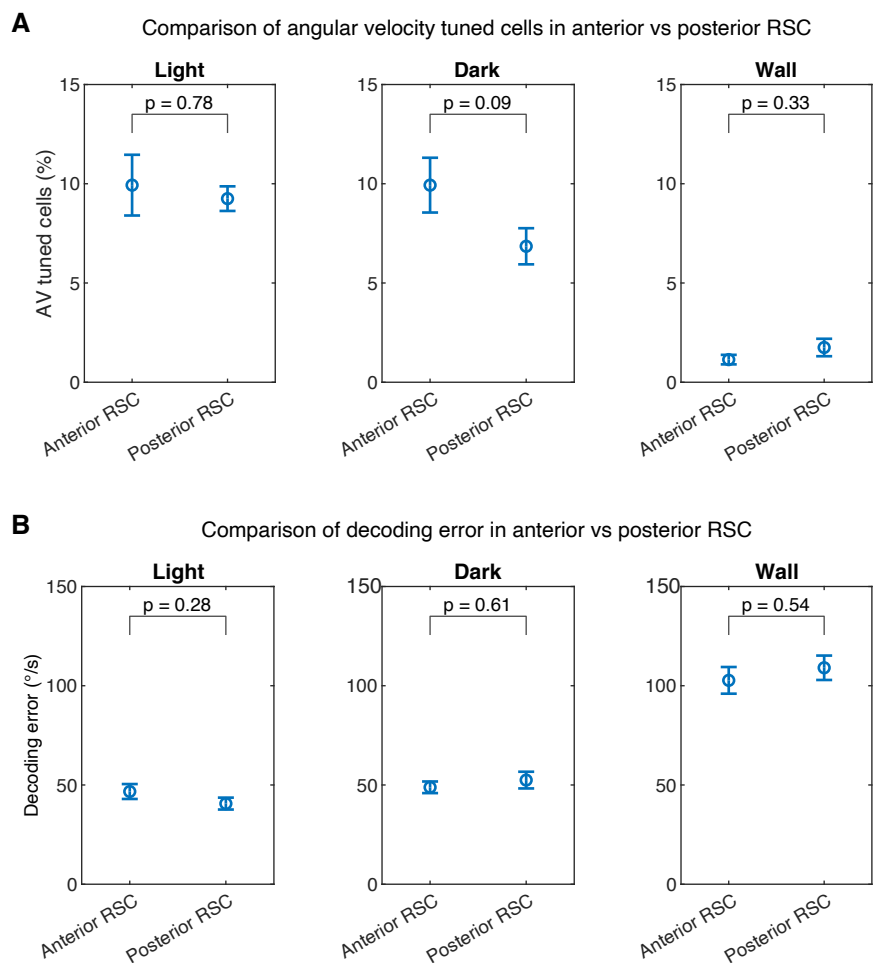
A

Comparison of angular velocity tuned cells in anterior vs posterior RSC

B

Comparison of decoding error in anterior vs posterior RSC

Figure S7. Comparison of anterior and posterior RSC. (Related to figure 7)

(A) Percentage of angular velocity tuned cells for the three different stimulus conditions (average ± s.e.m). Coordinates of anterior RSC, -1.64 to -2.5 mm; posterior RSC, -2.5 to -4.07 mm.

(B) Decoding error for the different stimulus conditions (average ± s.e.m). Statistical comparison between regions: Wilcoxon ranksum test. Number of sessions per condition and region: Anterior, light: 7 mice, 8 sessions; posterior, light: 6 mice, 7 sessions; anterior, dark: 7 mice, 8 sessions; posterior, dark: 6 mice, 7 sessions; anterior, wall: 6 mice, 6 sessions; posterior, wall: 4 mice, 5 sessions.
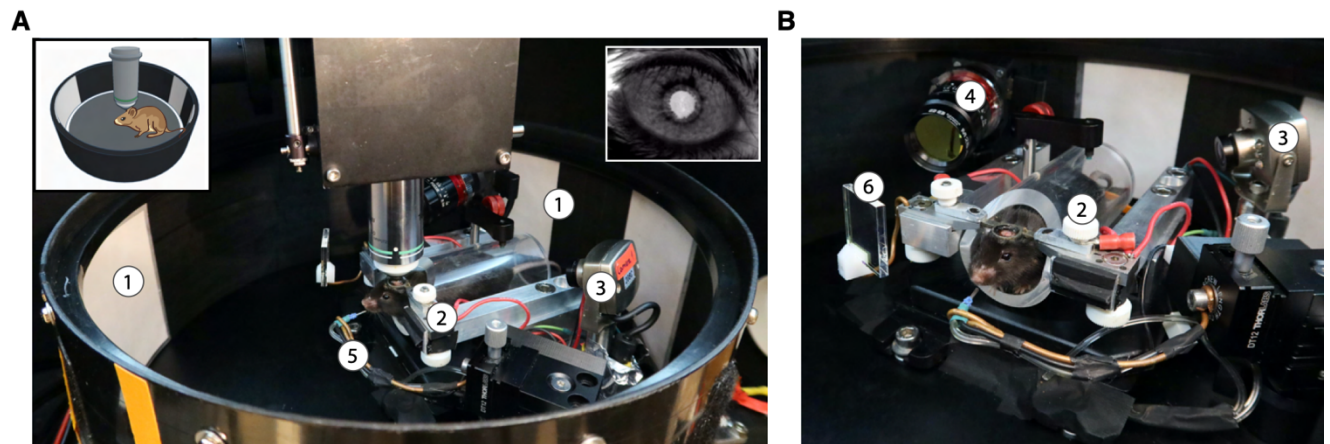
Figure S8. **Photographs of the setup. (Related to STAR methods)**

(A) Overview of the mouse in the rotation arena.

(B) Close-up of the mouse. 1 – Visual Cues, 2 – Mouse fixation frame, 3 – Body camera, 4 – Pupil camera, 5 – Lick spout, 6 – Infrared "hot" mirror.
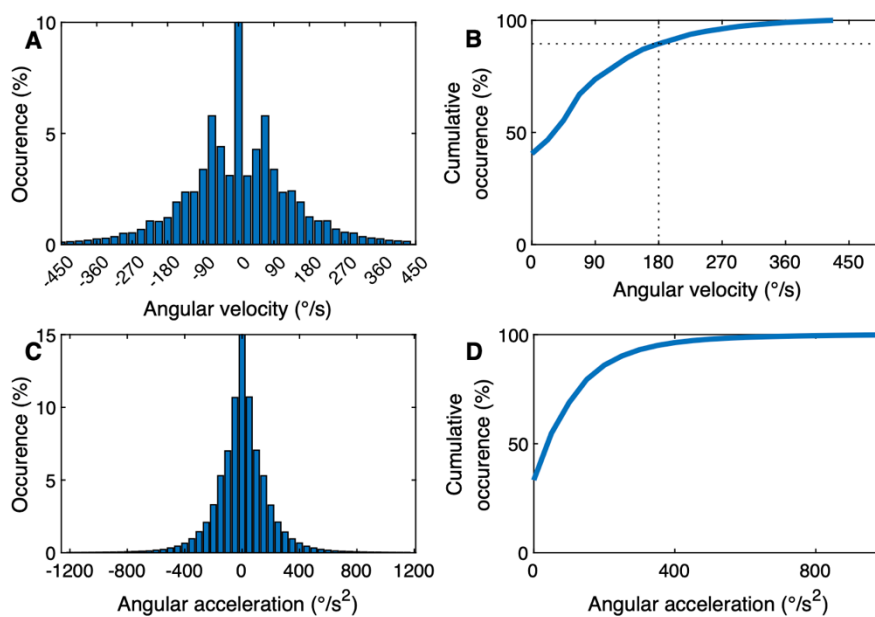

Figure S9. AHV and acceleration recorded from freely moving mice. (Related to *STAR methods*)

(A) Histogram of AHV.

(B) Cumulative histogram shows that 90 % of angular movements are below 180 °/s.

(C) Histogram of angular head acceleration.

(D) Cumulative histogram of angular head accelerations. Data kindly provided by Jean Laurens.
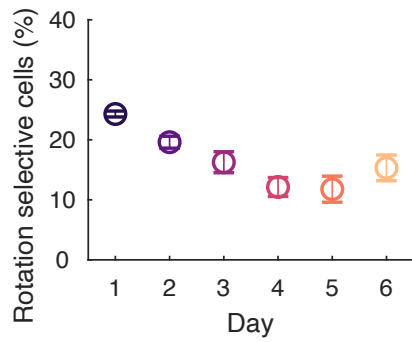
Figure S10. Percentage of rotation-selective cells decreases over days. (Related to *STAR methods*)

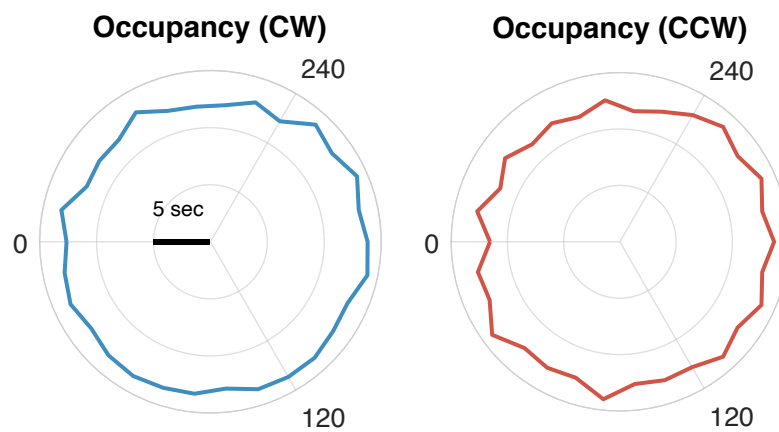Mean ± s.e.m. percentage of rotation-selective cells observed across 6 days (n = 4 mice).

Figure S11. Occupancy distribution. (Related to *STAR methods*)

Polar histogram of head direction occupancy during passive rotation for all CW trials (left) and all CCW trials (right)
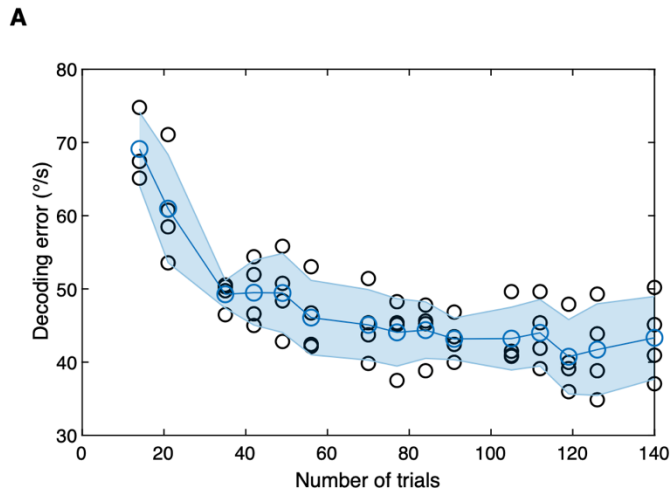
A

Figure S12. Decoding error as a function of trial number. (Related to *STAR methods*)

From a single session we took an increasing number of random trials to train the model. For each number, we picked a new set of random trials and determined the decoding error. Blue line is average ± s.e.m. (4 sessions from 3 mice).

p value (Rotation)

	V1	V2	RSC	PPC	M1-M2	S1
V1	1	0.71	0.28	0.24	0.14	0.06
V2	0.71	1	0.68	0.43	0.28	0.044
RSC	0.28	0.68	1	0.54	0.73	0.035
PPC	0.24	0.43	0.54	1	0.95	0.32
M1-M2	0.14	0.28	0.73	0.95	1	0.2
S1	0.06	0.044	0.035	0.32	0.2	1

p value (AHV)

	V1	V2	RSC	PPC	M1-M2	S1
V1	1	0.74	0.94	0.3	0.064	0.027
V2	0.74	1	0.53	0.24	0.13	0.016
RSC	0.94	0.53	1	0.26	0.029	0.0087
PPC	0.3	0.24	0.26	1	1	0.34
M1-M2	0.064	0.13	0.029	1	1	0.45
S1	0.027	0.016	0.0087	0.34	0.45	1

Figure S13. P-values of comparison for the percentage of CW/CCW cells (left) and AHV cells (right) across cortical areas. (Related to *STAR methods*)

Same data as in Figure 6B. See caption of Figure 6 for a detailed list of the numbers of mice for each plot.